Droplet Nucleation Processes Inside the Injectors of Supercritical Ethylene Jets

K.-C. Lin*
Taitech, Inc.
Beavercreek, Ohio 45430

Campbell Carter
Air Force Research Laboratory
Wright-Patterson AFB, Ohio 45433

Alec Sandy, Suresh Narayanan, Jan Ilavsky, Jin Wang
Argonne National Laboratory
Chicago, Illinois 60439

ABSTRACT

Nucleation processes and droplet size of condensed supercritical ethylene jets inside a rectangular injector were investigated, using the small-angle X-ray scattering (SAXS) technique. The experiment was conducted at the 8-ID beamline at the Argonne National Laboratory. The rectangular injector is equipped with diamond windows at various axial locations for X-ray access. Evolution of the internal flow properties, along with the effects of injection temperature and injector internal geometries on nucleation/growth processes, were investigated. It was found that the present injector design creates inconsistent flows, due to unexpected hardware issues, such as leakage and uneven junctions. Nonetheless, the ability of the SAXS technique to measure small incipient droplets generated from the homogeneous nucleation process was demonstrated in the present study. The incipient droplet size was measured in the range of 30-100 Å. The present efforts also demonstrate the capability to explore a highly dynamic supercritical ethylene jet inside an injector. The injection condition with an injectant temperature close to the critical temperature promotes nucleation upstream within the injector and generates large droplets. Also, the converging angle leading to the final nozzle passage affects the expansion process of the injected fluid and the onset of droplet formation inside the injector. No definite dependence on passage length could be obtained in the present study. Efforts to improve the injector design have been carried out. It is hoped that a new injector design, featuring an axisymmetric design made out of beryllium, will eliminate the present hardware-induced uncertainties.

*Corresponding author, Kuo-Cheng.Lin@wpafb.af.mil

INTRODUCTION

Injection of supercritical fluid for combustion in high-speed air-breathing propulsion systems has long been an important research area.[1] The use of endothermic hydrocarbon fuels as primary coolant around combustor components can potentially create thermally cracked hydrocarbon mixtures at supercritical conditions.[2] The supercritical fluid will behave differently from a gas or a liquid upon injection into the air-breathing combustor and may affect the combustion behavior of the engine, by liquid generation through homogeneous nucleation processes.[3]

The macroscopic structures of jets injected at supercritical conditions into a quiescent environment have been investigated in several studies.[3-5] The effects of injection conditions on the global appearance of the jets were characterized with shadowgraph images and the distribution profiles of the injected species at the downstream location were explored by Raman scattering. Figure 1 shows shadowgraph images of supercritical ethylene jets injected at two injection temperatures. The jet appearance changes from transparent at a high injection temperature (Fig. 1(a)) to optically opaque at a temperature close to the critical temperature (Fig. 1(b)). In the opaque jet, the fluid expands from the supercritical state into a two-phase thermodynamic region in the sub-critical state. Droplet nucleation and growth are initiated during this expansion process to generate a high density of small droplets within the plume. The study of Lin et al.[3] shows that the nucleation process can readily occur inside the injector (see Fig. 2). Further investigation of the liquid condensation process during the injection of supercritical fluid, however, was limited by the capability of conventional diagnostic techniques.

Recently, the small angle X-ray scattering (SAXS) technique available at the 8-ID beamline at the Argonne National Laboratory was utilized to characterize droplet properties inside condensed ethylene jets.[6] It was found that the SAXS technique is capable of measuring droplet size and liquid content inside a highly dynamic dense jet. The droplet size inside a condensed supercritical ethylene jet is on the order of 50-200 nm (500-2000 Å), which is smaller than that generated from industrial atomizers. Figure 3 (from Ref. [6]) illustrates the typical droplet size distribution. This is the first time that droplet size inside a highly dynamic condensed ethylene jet has been measured. While these observations are helpful for the characterization of droplet properties and liquid content inside a condensed ethylene jet outside the injector, the fundamental processes of droplet nucleation and subsequent droplet growth cannot be understood without probing the flow structures inside the injector.

In view of these observations, the objectives of this study are 1) to identify the onset of the nucleation process, 2) to measure the size of incipient droplets, and 3) to characterize droplet size evolution inside the injector. A 2-D injector equipped with diamond windows was designed and fabricated for SAXS measurements.

EXPERIMENTAL METHODS

Apparatus

The experiment was conducted at the 8-ID beamline at the Argonne National Laboratory. Pure ethylene (99.5%) at the desired temperature and pressure was injected into a chamber filled with nitrogen. The apparatus consists of an accumulator, a heating/chilling unit, a section of heat exchange tube, a solenoid valve, an injector, and the injection chamber. The chamber is equipped with two Kapton windows opposite to each other that provide high X-ray transmittance and low scattering, and two conventional optical windows that allow for visual inspection of injection. A simple schematic illustration of the experimental setup is shown in Fig. 4.

In test preparations, the well-purged and evacuated accumulator was first filled with ethylene. The filled accumulator was then pressurized, using nitrogen, to 5.15 MPa (750 psia), which is higher than the critical pressure of pure ethylene, P_c = 5.04 MPa (733.54 psia). Ethylene was then introduced into the heat exchanger to gradually reach the desired injection temperature. A heating/chilling unit controlled the temperature of ethylene glycol, used as the heat exchange medium, which flowed inside the annular passage of the heat exchanger. For the present study, the injection temperature, which was measured immediately upstream of the injection nozzle, was maintained between 283 K (T_r=1.00) and 306 K (T_r=1.08). The critical temperature for ethylene is T_c=282.4 K.

Before injection was begun, the injection chamber was flushed with nitrogen to remove oxygen and then pressurized with nitrogen to 137 kPa (20 psia). Once the test fluid reached the desired temperature, a solenoid valve with a response time of 150 ms was opened for about 5-10 s to charge the test fluid into the injection chamber. Due to the transient behavior of the jet, data obtained during the first 2 seconds of injection were discarded. With a further assessment on the injection transients, the scattering intensity profile obtained at 4.5 seconds after the initiation of injection was selected for discussion in the present study.

The injection chamber, which has an internal volume of 136 liters, was connected to the exhaust system through a venturi vacuum pump, which was used to quickly minimize the pressure rise inside the injection chamber. Nevertheless, an increase in

chamber pressure of up to 20% was observed over the course of injection. Since the ethylene jet is expected to be choked at the injector exit, however, the pressure increase in the injection chamber does not affect the flow structure inside the injector.

Injection Nozzles

Ten stainless steel, rectangular nozzles with various final passage lengths (L) and converging angles (θ) were used in the present study. Key parameters of each nozzle are tabulated in Table 1. Each nozzle begins with a rectangular passage (a width of 7.0 mm and a depth (D) of 1.0 mm), followed by a converging section (converging angle specified in Table 1), which leads to the final passage. The final passage has a small converging angle of 2 degrees, which will ensure that the choke point can occur only at the nozzle exit, which has an exit dimension of 1.0 mm by 1.0 mm. All transition corners are contoured to avoid any undesired flow separation.

The diamond windows were strategically placed at various locations along the injector axis for X-ray access. Single crystal diamond with a thickness of 0.3 mm (0.012") and a diameter of 3.8 mm (0.15") was selected to provide reasonable X-ray transmission and reasonably low scattering. For probing close to the nozzle exit, arch-shaped diamond windows were used to ensure a flush-exit surface. The photograph and schematic shown in Fig. 5 illustrate the internal geometry of Injector #1, along with Window #0 adjacent to the nozzle exit. Due to the limitations on available diamond window sizes and available space to accommodate window flanges, only one window location at a time can be used. For the present study, Window #0 was used to probe the region with $x \geq -2.9$ mm ($x=0$ at the nozzle exit and $x<0$ inside the injector), which covers the passage region near the nozzle exit for all injectors in Table 1. Window #1 was used to cover the region further upstream with $x \leq -3.4$ mm, as illustrated in Fig. 6. For the injector configuration with a relatively long L/D, different window blocks (Windows #2, #3, etc.) with desired X-ray probing ranges along the injector axis were designed and fabricated. The entire injector assembly was designed to ensure proper sealing at high injection pressures. As will be shown later, sealing the thin windows is challenging.

Instrumentation and Data Reduction

A monochromatic, 0.17×0.17 mm^2 X-ray beam with a photon flux of $\sim 10^{11}$ s^{-1} in the 8-ID beamline was directed through the injector. The distance between the injector axis and the detector was maintained at 3.45 m, in order to capture the scattering pattern at smaller scattering angles from potential larger droplets. A photon-counting 2-D array X-ray detector (PILATUS detector) was utilized to capture the forward-scattered X-ray photons. A total of 6 images were obtained for each injection condition. Figure 7 shows typical small-angle scattering raw image for a highly-condensed supercritical ethylene jet. Details on data reduction to convert the measured scattering intensity to droplet size and liquid volume fraction can be found in Ref. [6].

RESULTS AND DISCUSSION

Incipient Droplet Size from Homogeneous Nucleation

Figure 8 shows the measured and calculated scattering intensity profile, calculated droplet size, and calculation residual at x= -3.4 mm for Injector #6 with $T_{chiller}$=284 K (11 C). This scattering intensity profile shows that the curve fitting process can be performed over the entire Q range to give a size distribution profile. Please note that the fitted intensity profile overlaps fairly well with the measured intensity profile (shown beneath the measured profile in Fig. 8). The calculation residual is also fairly low, except at the ends of the measured profile. The calculated droplet size is between 30-200 Å with a peak of around 75 Å for the test condition in Fig. 8. These droplets may be the incipient droplets generated from the homogeneous nucleation process. Thus, the ability of the SAXS technique to measure small incipient droplets generated from the homogeneous nucleation process is demonstrated in the present study. Also, the present efforts demonstrate, for the first time, the ability to explore a highly dynamic supercritical ethylene jet inside an injector.

Evolution Along Injector Axis:

Figure 9 shows the intensity profiles at six axial locations inside Injector #1. Window #1 was used to probe the region around the transition of the internal contour leading to the final nozzle passage ($x \leq -3.4$ mm). Window #0 was used to probe the final passage region near the nozzle exit ($x \geq -2.9$ mm). As can be seen in Fig. 9, there is a significant evolution in scattering intensity profiles along the injector axis within the probing area of Window #1. From x= -5.4 mm to -4.4 mm, a small quantity of large droplets is generated within the X-ray line of sight, as is seen from the low scattering intensity at low Q. Of course, it is impossible to tell whether the large droplets are located along the injector axis or close to the injector wall. The intensity at the high Q regime ($Q>0.02$ Å^{-1}) remains the same at both locations, indicating the same population of small droplets.

Figure 10(a) shows that small scatterers with diameters on the order of 20-50 Å are obtained, using a Q range of 0.03-0.09 Å^{-1} for curve fitting, at both the x= -4.4 and -5.4 mm locations. These small scatterers are believed to be incipient ethylene droplets. As the probing location is moved from x= -4.4 mm to -3.4

mm, a significant change in scattering intensity profiles is observed. At the x= -3.4 mm location, the scattering profile exhibits a higher scattering intensity at low Q and a reduction in the scattering intensity at high Q ($Q>0.05$ Å^{-1}). The significant difference in scattering intensity profiles indicates an apparent change in flow properties. Based on the intensity profile alone, it appears that there is a reduction in the number of small droplets (corresponding to high Q), probably due to coalescence and formation of larger droplets. The presence of large droplets (corresponding to low Q) is also quite evident. At x= -3.4 mm, the calculated droplet size using the entire Q range is between 40 and 200 Å. This size range is larger than that at the upstream x= -4.4 and -5.4 mm locations, probably due to droplet growth/coalescence.

As the probing location is moved to Window #0 at the downstream location, the scattering intensity profiles exhibit dramatic changes from those obtained with Window #1. It appears that more large droplets are generated at downstream locations. The calculated droplet size distributions in Fig. 10(b) (linear scale) indicate that the droplet size evolves from 500-1500 Å with a peak around 1200 Å at the x= -2.9 mm location to 700-2700 Å with a peak around 1500 Å at the x= -0.9 mm location.

The dramatic increase in droplet size from 40-200 Å at the x= -3.4 mm location to 500-2700 Å at the x= -2.9 mm location cannot be reasonably explained by droplet growth alone. The sudden increase in droplet size prompts a further examination of the test conditions. Table 2 lists the injection conditions for Fig. 9. While the injection temperature is fairly consistent within the temperature control range, the injection pressure and the measured ethylene mass flow rate exhibit significant variations between window locations. The ethylene mass flow rate for Injector #1 with Window #0 installed was higher, indicating a possible leakage around Window #0 or a difference in flow passage dimension between window assemblies. This hardware-induced discrepancy, however, could not be resolved during the experiment period at the Argonne National Laboratory. Consequently, it must be assumed that the flow property evolution can best be evaluated using a single window assembly, with the presumption that the impact of any possible leakage is consistent for a given window. The exact mechanisms for the appearance of a significant number of large droplets in the flow behind Window #0 are unknown at this stage.

Effects of Injection Temperature:

The effect of T_{inj} on flow properties is demonstrated in Fig. 11. All six test conditions were conducted within the same field of view of Window #1, using Injector #1 with $T_{chiller}$=287 K (14 C) or 296 K (23 C). The injection conditions and the measured ethylene mass flow rate are listed in Table 3. It appears that the injection conditions with $T_{chiller}$=287 K (14 C) exhibit a slightly higher ethylene mass flow rate, due to the temperature-related density difference, so it is concluded that the results are not affected by the hardware assembly.

The profiles in Fig. 11(a) show that the scattering intensity increases as the injectant temperature decreases at the same probing location, probably due to the increased probability of homogeneous nucleation. At both the x= -4.4 and -5.4 mm locations, the injection conditions with $T_{chiller}$=296 K (23 C) do not generate large droplets to produce scattering at low Q. The significantly higher scattering intensity levels at low Q with $T_{chiller}$=287 K (14 C) indicate that large droplets already exist at both probing locations. Based on this observation, it is evident that the injection condition with an injectant temperature close to the critical temperature promotes early (upstream) generation of large droplets. The calculated size distribution profiles in Fig. 11(b) at both measurement locations show that the droplet size and volume fraction increase slightly for the test condition with $T_{chiller}$=287 K (14 C). Apparently, the injection temperature also affects the size and population of small droplets. The size range for the small droplets is from 20 to 70 Å. The size of the large droplets with $T_{chiller}$=287 K (14 C) could not be resolved by curve fitting within the low Q range at both probing locations.

At the x= -3.4 mm location, the scattering intensity profiles for both injectant temperatures in Fig. 11(a) exhibit similar characteristics, i.e., high scattering intensity at the low Q regime and significant low scattering intensity at the high Q regime, with the $T_{chiller}$=296 K (23 C) condition showing a lower intensity level. The calculated size distributions show that the $T_{chiller}$=287 K (14 C) condition produces more large droplets than does the $T_{chiller}$=296 K (23 C) condition.

To summarize the effect of injectant temperature on droplet generation, injectant temperature close to the critical temperature promotes early occurrence of nucleation, which allows a longer residence time for nuclei to grow into large droplets inside the injector. This conclusion echoes the visual observations in Fig. 2.

Effects of Injector L/D:

The effect of injector internal geometry on the nucleation process was investigated in terms of the convergence angle leading to the final nozzle passage (θ) and the passage length (L/D). Figure 12 shows the scattering intensity profiles within the field of view of Window #1 for Injectors #1 (θ=180°, L/D=4) and #3 (θ=180°, L/D=8) at the same T_{inj} and P_{inj} (see Table 4).

The X-ray probing locations related to the internal contours of both injectors are illustrated in Fig. 13. Injector #3 was expected to have a slightly lower ethylene flow rate due to its relatively long passage length. The measurements, however, show negligible difference in all tabulated values in Table 4, probably due to the relatively large nozzle exit dimension (1.0 mm × 1.0 mm) and the small difference in L/D.

As can be seen in Fig. 12, the injector with a long L/D tends to generate higher scattering intensity profiles at the same injection condition and the same distance from the injector exit. Injector #1 does not generate large droplets at either the x= -4.4 or the -5.4 mm locations, as illustrated in the corresponding size distribution profiles in Fig. 14(a). Only small droplets with the size range of 20-55 Å exist at both locations. The transition from the presence of small droplets to the presence of large droplets takes place, once again, between x= -3.4 and -4.4 mm for this injector. For Injector #3 with an L/D of 8, large droplets already exist at the x= -5.4 mm location, indicating that the nucleation process takes place further upstream. These large droplets could not be resolved in the size calculation shown in Fig. 14(a). A significant change in scattering intensity profile takes place between x= -5.4 and -4.4 mm, indicating the occurrence of a significant growth/coalescence process within the 1.0 mm distance. At both the x= -4.4 and -3.4 mm locations for Injector #3, there is no significant difference in scattering intensity profiles for $Q<0.05$ $Å^{-1}$, indicating the presence of large droplets with similar size range and population. This is shown by the calculated droplet sizes in Fig. 14(b), where droplets smaller than 100 Å are omitted for the sake of clarity. Fairly large droplets in the range of 300-3000 Å are found. Consistent injection conditions for both injectors equipped with Window #0, unfortunately, could not be obtained in the present study, due apparently to leakage. Scattering characteristics at regions further downstream could not be examined to understand the growth process for this pair of injectors.

Figure 15 shows another set of test conditions to illustrate the effect of injector L/D. Injector #7 with L/D=4 and Injector #10 with L/D=12 were tested with Window #0 at the same chiller temperature and pressure inside the heat exchanger. Figure 16 shows the relative location between Window #0 and the internal contours of Injectors #7 and #10. The actual injection conditions in Table 5 show that a high ethylene mass flow rate can be injected through Injector #7, due to its short passage length and resultant small pressure drop. With the assumption that there is no leakage, uneven junction, or surface roughness difference to trigger unexpected mechanisms for nucleation and growth, Figure 15 shows that Injector #10 with L/D=12 generates a smaller number of droplets on the order of 1000 Å and produces larger droplets for those droplets on the order of 100 Å than Injector #7 with L/D=7 does near the injector exit. It can thus be inferred that a long residence time offered by an injector with a larger L/D may not proportionally promote the growth/coalescence processes. At a given injection condition, ethylene inside the injector with a long L/D undergoes the initial expansion process through the convergent section earlier, and thus the nucleation process takes place earlier. It is expected that the relatively long L/D should provide a longer residence for nuclei to grow into large droplets before exiting the nozzle. The observations in Fig. 15, however, contradict this general sense. Differences in heat transfer or expansion process experienced by the injectant may be the contributing mechanisms for the observed difference in droplet size. Based on the observation so far, no definite dependence of droplet diameter on passage length could be obtained in the present study.

Effects of Injector Convergence Angle:

Figure 17 shows the measured scattering intensity profiles and the corresponding size distributions for Injector #6 (θ=60°), #7 (θ=120°), and #1 (θ=180°) within the field of view of Window #1. These selected injectors have the same final passage length and were operated at the same temperature and pressure inside the heat exchanger. The viewing area of Window #1 covers the transition region of the final passage, as illustrated in Fig. 18. The injection conditions listed in Table 6 show that the injection conditions are consistent among these three injectors. As can be seen from the scattering intensity profiles of Fig. 17, the configuration of Injector #6 promotes the early presence of large droplets, probably due to the expansion process induced by its long convergent section and gradual converging angle of 60°. For Injector #7, there is a lower scattering intensity level and no presence of large droplets within the field of view of Window #1. The scattering characteristics from Injector #1 with θ=180° exhibits indicates fewer large droplets than Injector #6 at both x= -5.4 and -4.4 mm locations, which are outside the transition section of the injector contour. At the x= -3.4 mm location, however, Injector #1 suddenly generates a higher scattering intensity with larger droplets on the order of 40-200 Å. Based on the observations so far, it appears that the injector convergence angle can affect the growth/coalescence processes. Due to a significant leakage associated with the Window #0 assembly for all three injectors, flow properties at the downstream locations could not be meaningfully compared.

The observation that Injector #6 promotes early nucleation but ultimately produces small droplets on the order of 100 Å (Fig. 17) and the observation that Injector #10 (with a long L/D) eventually generates droplets on the order of 1000 Å (Fig. 15), even though

the droplets are not of the same size class, highlights that residence time may not be the major contributing mechanism in generating large droplets. Instead, the expansion process experienced by the fluid should not be overlooked.

CONCLUSIONS

The structures of condensed supercritical ethylene jets inside a rectangular injector were explored using the small-angle X-ray scattering (SAXS) technique. The experiment was conducted at the 8-ID beamline at the Argonne National Laboratory. The rectangular injector is equipped with diamond windows at various axial locations for X-ray probing. Scattering intensity was measured and the corresponding size and population of droplets were calculated. Evolution of the internal flow properties, along with the effects of injection temperature and injector internal geometries on nucleation/growth processes, were investigated. It was found that the present injector design creates inconsistent flows for some injection conditions, probably due to leakage, uneven junctions, or wall surface roughness. Consequently, conclusions for some of the intended parametric comparisons could not be made with confidence. Findings of the present study are summarized below:

1. The ability of the SAXS technique to measure small incipient droplets generated from the homogeneous nucleation process was demonstrated. The measured incipient droplet size is in the range of 30-100 Å. The present efforts also demonstrate, for the first time, the capability to explore a highly dynamic supercritical ethylene jet inside an injector.

2. Populations of X-ray scatterers of two sizes were observed inside the injector. One population is on the order of 100 Å and is consistently present inside the injector. The other population is on the order of 1000 Å and is mainly present in the downstream region. These 1000 Å droplets are are suspected to be associated with the windows or the window assembly.

3. The injection condition with an injectant temperature close to the critical temperature promotes early occurrence of nucleation, which allows a greater residence time for nuclei to grow into large droplets.

4. Evidence that the nucleation/growth processes also depend on the injector contour is obtained in the present study. In particular, the converging angle leading to the final nozzle passage affects the expansion process of the injected fluid and, therefore, the onset of droplet presence inside the injector. No definite dependence on passage length could be obtained, however, in the present study.

In the course of post-test data analysis, it became clear that the injector hardware must be refined. An effort to explore the feasibility of making conventional axisymmetric injectors out of beryllium for the study of internal flow structures is currently underway. The relatively high X-ray transmittance of beryllium makes it a candidate for the present SAXS measurement technique. The same injector can also be utilized for the investigation plume structures outside the injector. More importantly, this new injector design would eliminate the present hardware-induced uncertainties to provide accurate answers to the above-mentioned open questions.

ACKNOWLEDGEMENTS

This work was sponsored by the AFRL/Propulsion Directorate under contract number FA856008D2844 (Contract monitor: Robert Behdadnia). Use of the Advanced Photon Source at Argonne National Laboratory was supported by the U. S. Department of Energy, Office of Science, Office of Basic Energy Sciences, under Contract No. DE-AC02-06CH11357. The authors would like thank Matt Streby, Steve Enneking, and Timothy Bulcher (Taitech, Inc.) for their assistance in hardware design, setup, and data acquisition.

REFERENCES

1. Edwards, T., “USAF Supercritical Hydrocarbon Fuels Interests,” AIAA Paper 93-0807, January 1993.
2. Edwards, T. and Anderson, S. D., “Results of High Temperature JP-7 Cracking Assessment,” AIAA Paper 93-0806, January 1993.
3. Lin, K.-C., Cox-Stouffer, S., Kennedy, P., and Jackson, T., “Expansion of Supercritical Methane/Ethylene Jets in a Quiescent Subcritical Environment,” AIAA Paper 2003-0483, January 2003.
4. Wu, P.-K., Shahnam, M., Kirkendall, K. A., Carter, C. D., and Nejad, A. S., “Expansion and Mixing Processes of Underexpanded Supercritical Fuel Jets Injected into Superheated Conditions,” *Journal of Propulsion and Power*, Vol. 15, No. 5, 1999, pp. 642-649.
5. Wu, P.-K., Chen, T. H, Nejad, A. S., and Carter, C. D., “Injection of Supercritical Ethylene into Nitrogen,” *Journal of Propulsion and Power*, Vol. 12, No. 4, 1996, pp. 770-777.
6. Lin, K.-C., Carter, C., Sandy, A., Narayanan, S., Ilavsky, J., and Wang, J., “Investigation of Droplet Properties of Supercritical Ethylene Jets Using

Table 1 Geometries of the injection nozzles

Injector	**1**	**2**	**3**	**4**	**5**	**6**	**7**	**8**	**9**	**10**
D (mm)	1.0	1.0	1.0	1.0	1.0	1.0	1.0	1.0	1.0	1.0
L/D	4	2	8	4	8	4	4	6	8	12
θ	180	180	180	90	90	60	120	120	120	120

Table 2 Injection conditions for the test conditions in Fig. 9.

x (mm)	P_{inj} (MPa)	T_{inj} (K)	P_r	T_r	mdot(g/s)
-5.4	5.19	284.9	1.03	1.01	13.5
-4.4	5.18	284.9	1.03	1.01	13.2
-3.4	5.25	284.7	1.04	1.01	13.5
-2.9	5.05	283.7	1.00	1.00	20.7
-1.9	5.05	283.8	1.00	1.01	20.7
-0.9	5.06	284.0	1.00	1.01	20.5

Table 3 Injection conditions for the test conditions in Fig. 11.

$T_{chiller}$ (C)	x (mm)	P_{inj} (MPa)	T_{inj} (K)	P_r	T_r	mdot(g/s)
14	-5.4	5.19	284.9	1.03	1.01	13.5
14	-4.4	5.18	284.9	1.03	1.01	13.2
14	-3.4	5.25	284.7	1.04	1.01	13.5
23	-5.4	5.20	293.0	1.03	1.04	12.2
23	-4.4	5.19	293.0	1.03	1.04	12.3
23	-3.4	5.18	292.9	1.03	1.04	12.3

Table 4 Injection conditions for the test conditions in Fig. 12.

Injector	x (mm)	P_{inj} (MPa)	T_{inj} (K)	P_r	T_r	mdot(g/s)
#1	-5.4	5.20	290.9	1.03	1.03	12.6
#1	-4.4	5.20	291.0	1.03	1.03	12.6
#1	-3.4	5.21	291.1	1.03	1.03	12.5
#3	-5.4	5.21	290.9	1.03	1.03	12.4
#3	-4.4	5.22	291.0	1.03	1.03	12.5
#3	-3.4	5.22	291.1	1.03	1.03	12.8

Table 5 Injection conditions for the test conditions in Fig. 15.

Injector	x (mm)	P_{inj} (MPa)	T_{inj} (K)	P_r	T_r	mdot(g/s)
#7	-0.9	5.03	290.9	1.01	1.03	20.0
#7	-1.9	5.05	290.7	1.01	1.03	19.6
#7	-2.9	5.04	290.5	1.01	1.03	19.6
#10	-0.9	5.16	291.2	1.03	1.03	13.4
#10	-1.9	5.19	291.0	1.03	1.03	13.2
#10	-2.9	5.18	290.9	1.03	1.03	13.0

Table 6 Injection conditions for the test conditions in Fig. 17.

Injector	θ (°)	x (mm)	P_{inj} (MPa)	T_{inj} (K)	P_r	T_r	mdot(g/s)
#6	60	-5.4	5.16	284.7	1.02	1.01	13.4
#7	120	-5.4	5.18	285.2	1.03	1.01	13.2
#1	180	-5.4	5.19	284.9	1.03	1.01	13.5
#6	60	-4.4	5.17	284.5	1.03	1.01	13.4
#7	120	-4.4	5.18	285.4	1.03	1.01	13.2
#1	180	-4.4	5.18	284.9	1.03	1.01	13.2
#6	60	-3.4	5.22	284.3	1.04	1.01	13.3
#7	120	-3.4	5.19	285.9	1.03	1.01	13.9
#1	180	-3.4	5.25	284.7	1.04	1.01	13.5

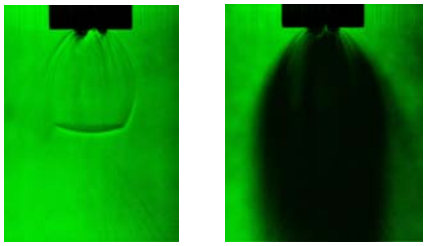

T_{inj}(K) 308 284.7

Figure 1 Shadowgraph images of supercritical ethylene jets injected at various temperatures into a quiescent chamber filled with nitrogen at 137 kPa (20 psia). Injection pressure is 5.15 MPa (750 psia). Images are from Ref. [6].

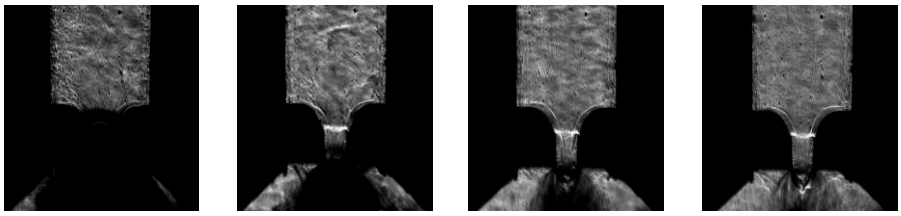

T_{inj}/T_c 1.00 1.01 1.03 1.08

Figure 2 Shadowgraph images of ethylene jets in a transparent injector. D=1.0 mm, L=4 mm, P_{inj}= 5.14 MPa, P_{chm}= 0.14 MPa. Images are from Ref. [3].

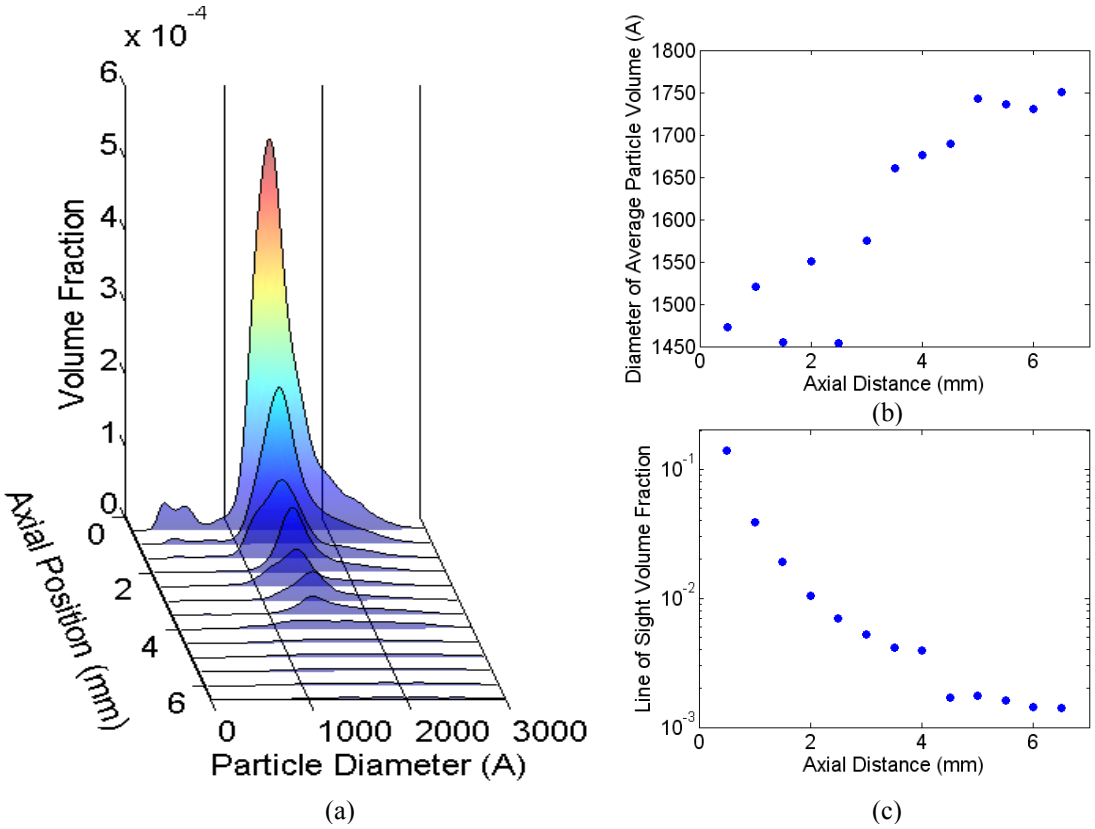

Figure 3 Line-of-sight distributions for droplet diameter and liquid volume fraction for a supercritical ethylene jet at various axial locations. Injector #4, d=1.0 mm, T_{inj}=283.1 K. (a) Droplet size vs. liquid volume fraction distribution profiles, (b) Axial distribution for the average droplet size weighted by the liquid volume fraction, (c) Axial distribution for the total liquid volume fraction. From Ref. [6]

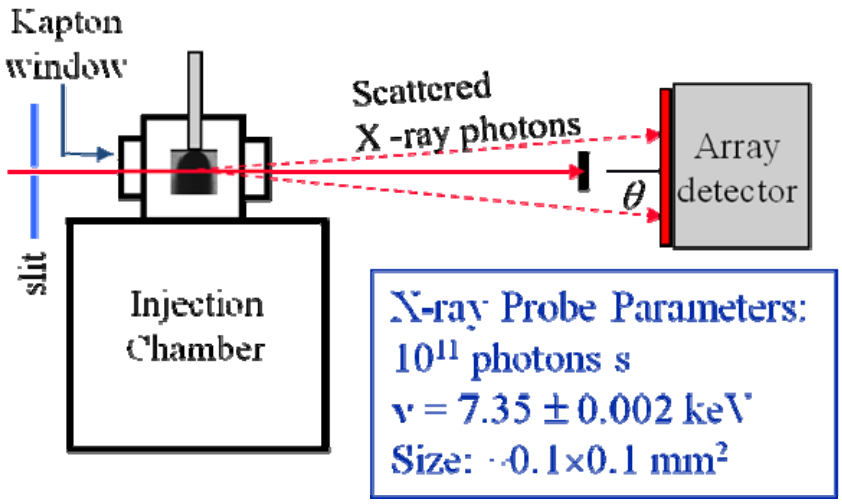

Figure 4 Schematic of chamber and optical layout

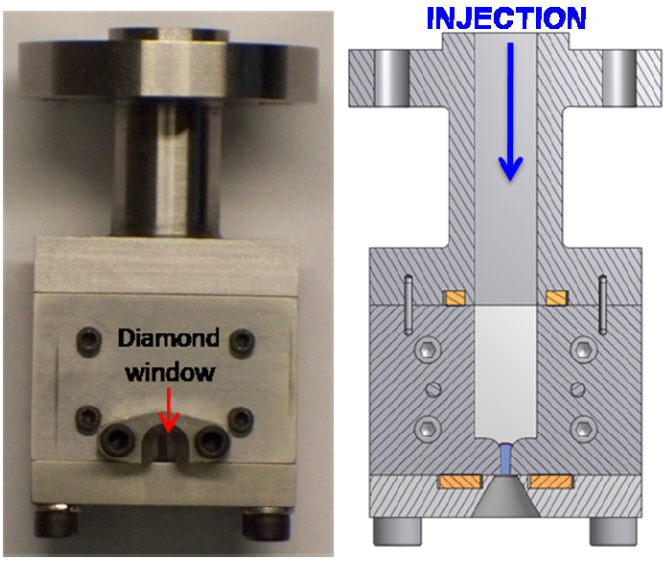

Figure 5 Photo and schematic to illustrate the 2-D injector equipped with diamond film windows. Contour of Injector #1 and Window #0 are shown.

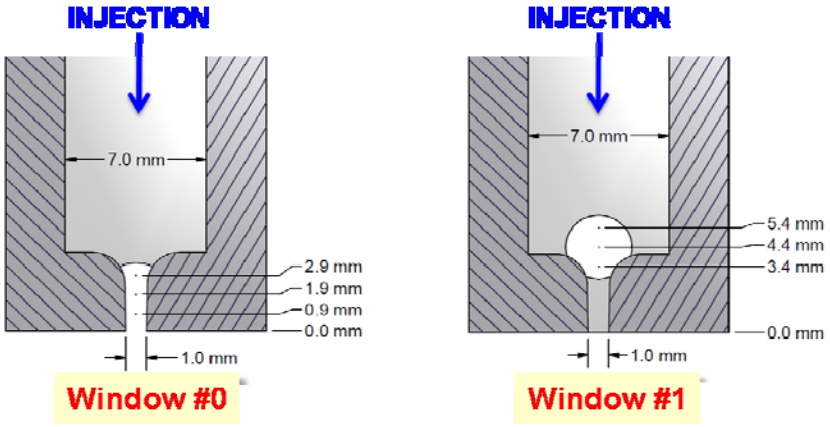

Figure 6 Schematic to illustrate the window locations for Injector #1.

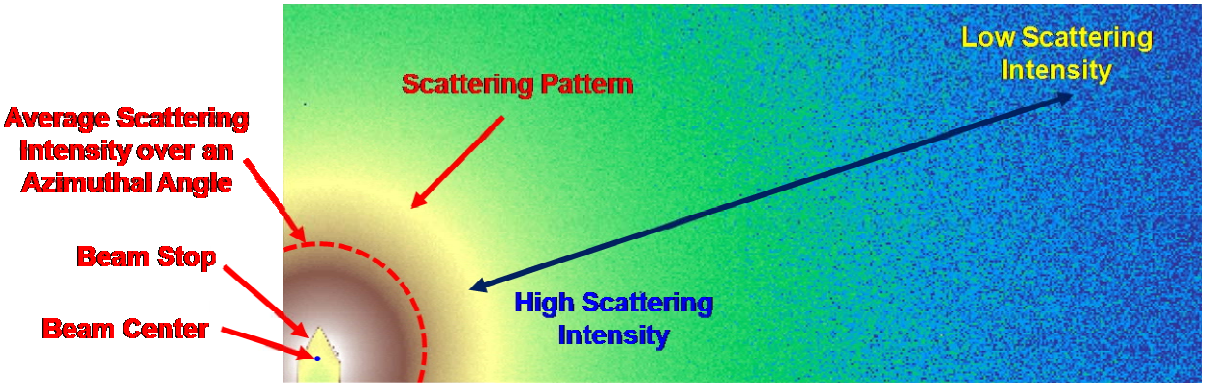

Figure 7 The typical small-angle scattering image for a highly-condensed supercritical ethylene jet.

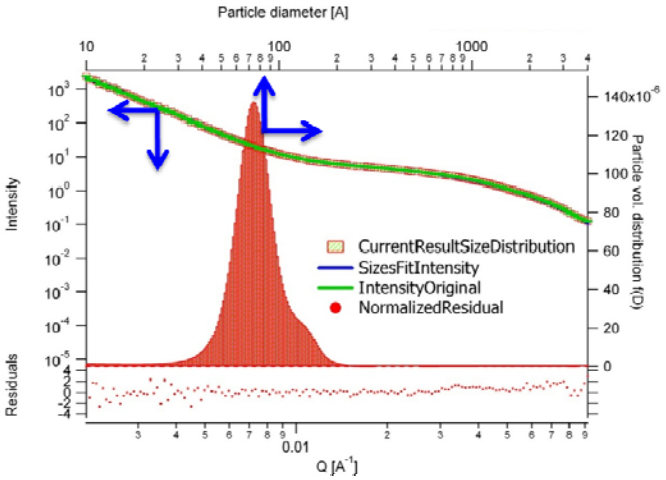

Figure 8 Measured (green line) and fitted (blue line, overlapped beneath the green line) scattering intensity profile, calculated droplet size distribution (green bar with red border, appear as red column), and the calculation residual (red dots) at x= -3.4 mm for Injector #6 operated at $T_{chiller}$=284 K (11 C).

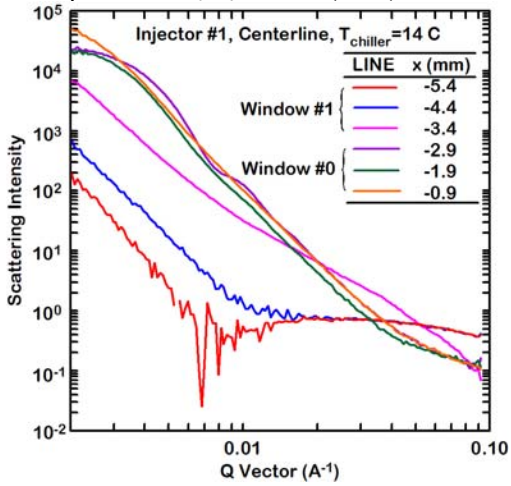

Figure 9 Scattering intensity profiles measured at different axial locations along the centerline of Injector #1. $T_{chiller}$=287 K (14 C).

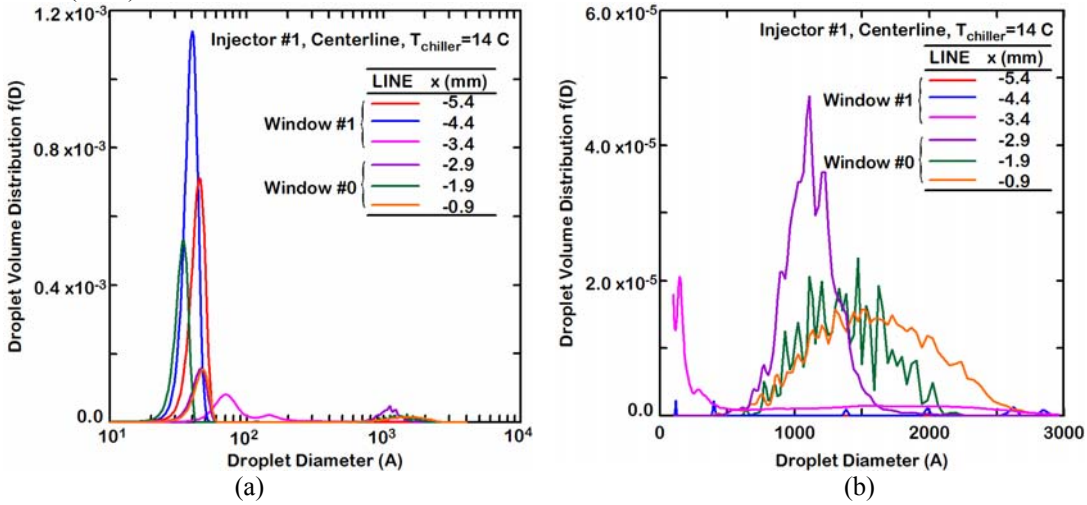

Figure 10 The calculated droplet size distributions (a) over the entire measureable droplet size range in log scale and (b) over the range excluding small diameters (<100 Å) in linear scale at different axial locations along the centerline of Injector #1. $T_{chiller}$=287 K (14 C).

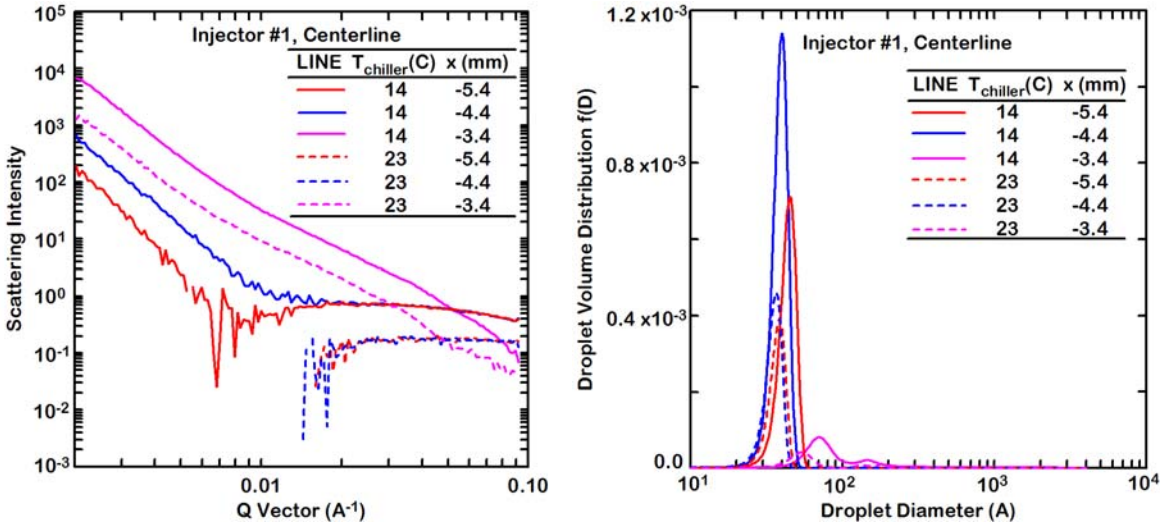

(a) (b)

Figure 11 (a) Scattering intensity profiles and (b) calculated droplet diameter for two $T_{chiller}$ (287 K (14 C) and 296 K (23 C)) at different axial locations along the centerline of Injector #1. Window #1 was installed.

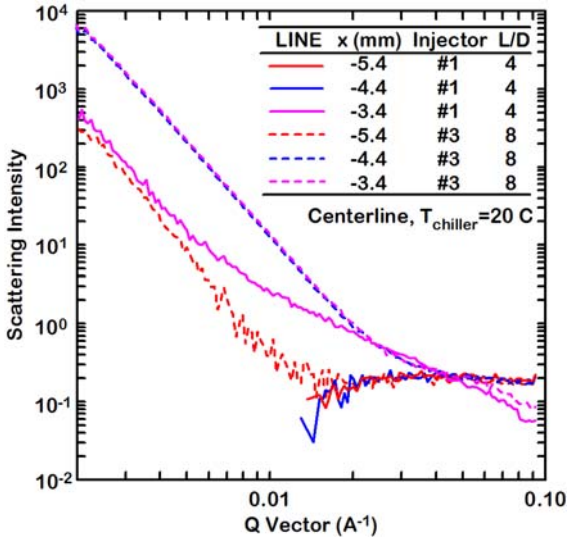

Figure 12 Scattering intensity profiles measured at different axial locations along the centerlines of Injectors #1 (L/D=4) and 3 (L/D=8). θ=180°, $T_{chiller}$=293 K (20 C), Window #1.

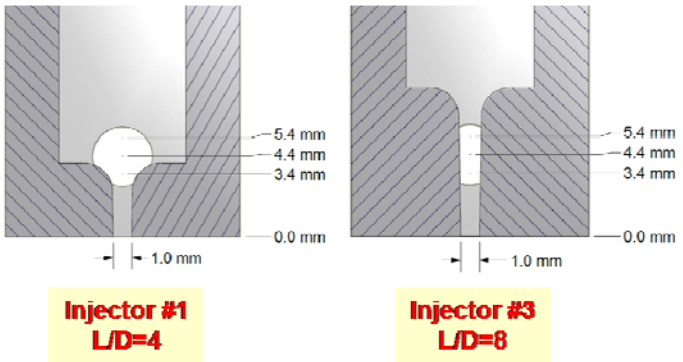

Figure 13 Schematic to illustrate the Window #1 location with respect to the Injector #1 and #3 configurations.

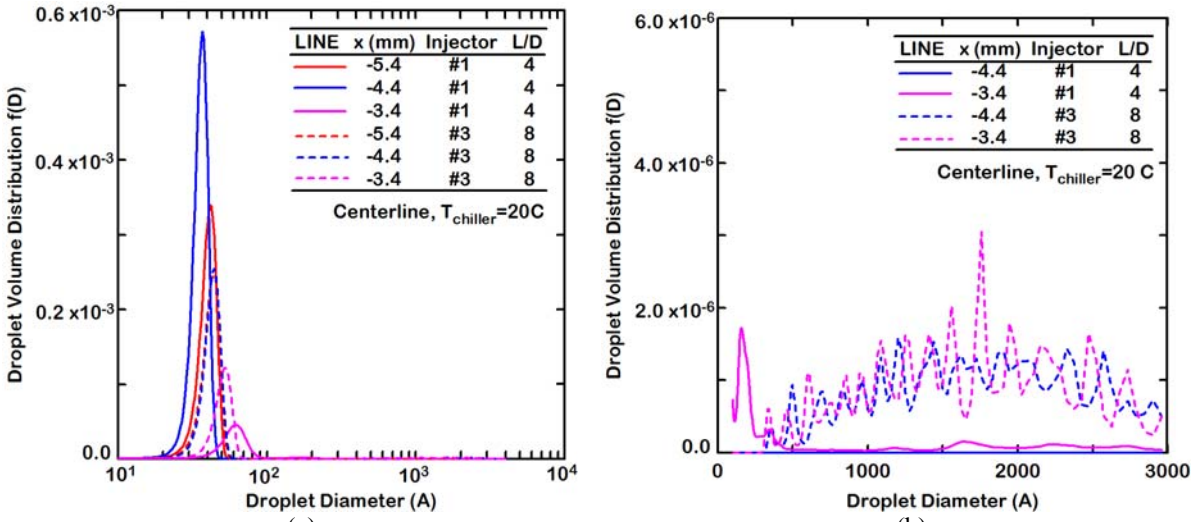

Figure 14 The calculated droplet size distributions (a) over the entire measureable droplet size range in log scale and (b) over the range excluding small diameter (<100 Å) in linear scale at different axial locations along the centerlines of Injectors #1 (L/D=4) and #3 (L/d=8). θ=180°, $T_{chiller}$=293 K (20 C), Window #1.

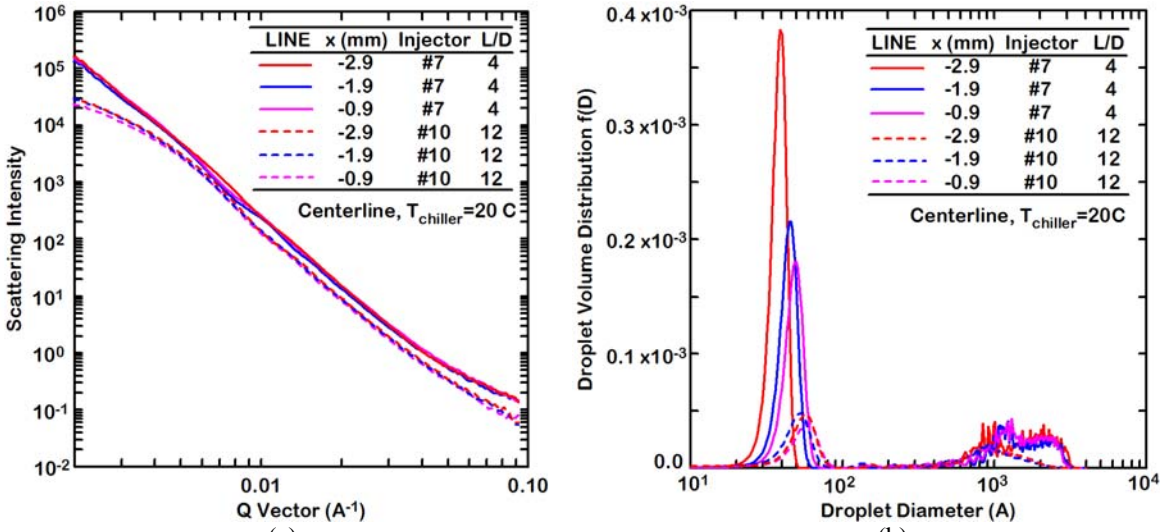

Figure 15 (a) Scattering intensity profiles and (b) calculated droplet diameter at different axial locations along the centerlines of Injectors #7 (L/D=4) and 10 (L/D=12). θ=120°, $T_{chiller}$=293 K (20 C), Window #0.

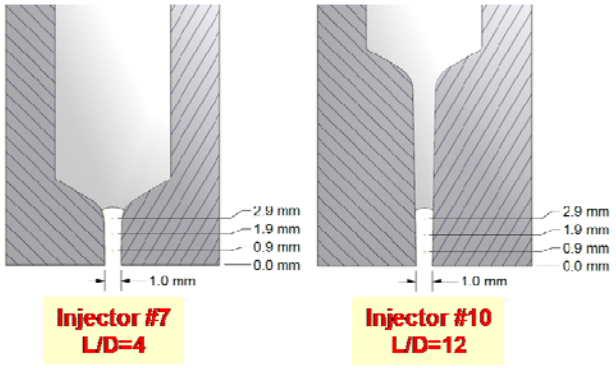

Figure 16 Schematic to illustrate the Window #0 location with respect to the Injector #7 and #10 configurations.

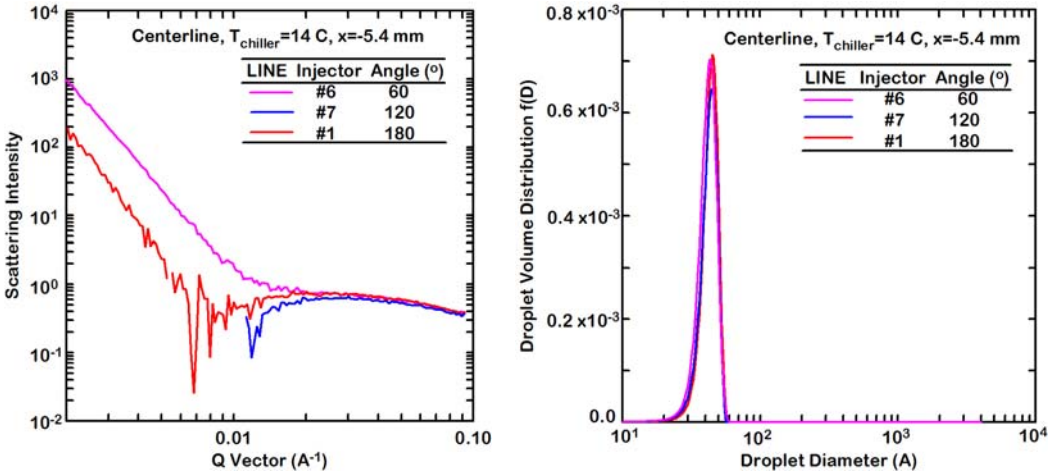

(a)

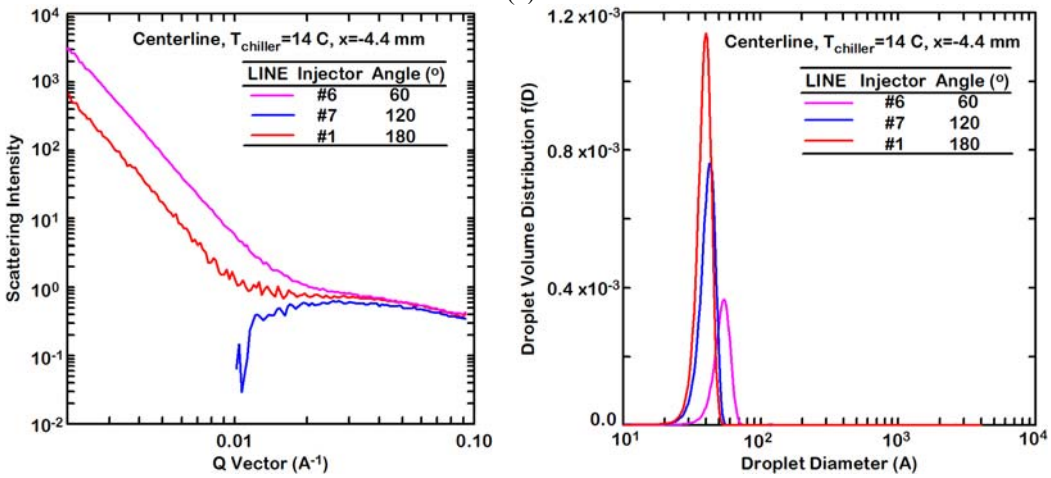

(b)

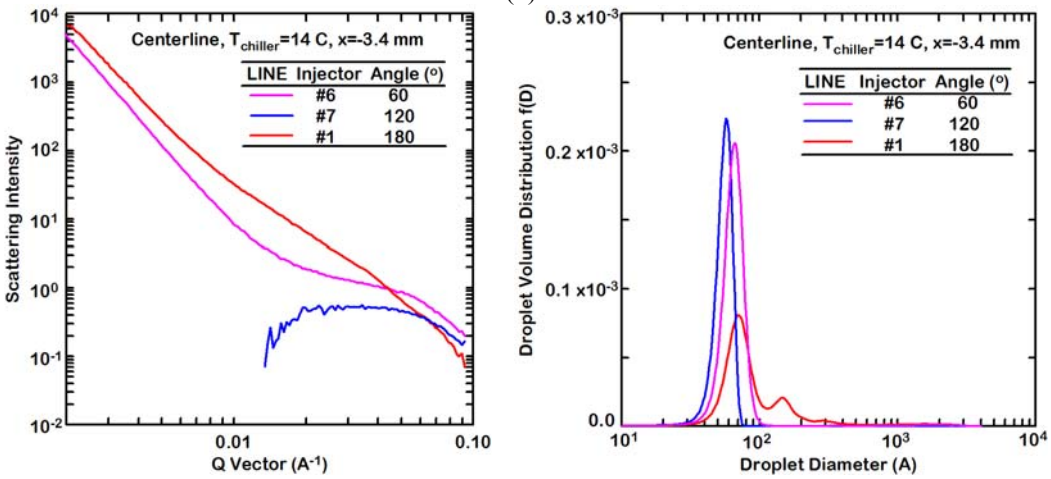

(c)

Figure 17 Scattering intensity profiles and calculated droplet diameter, to show the effect of injector convergence angle at different axial locations along the injector centerlines. (a) x=-5.4 mm, (b) x=-4.4 mm, (c) x=-3.4 mm.. $T_{chiller}$=287 K (14 C), Window #1.

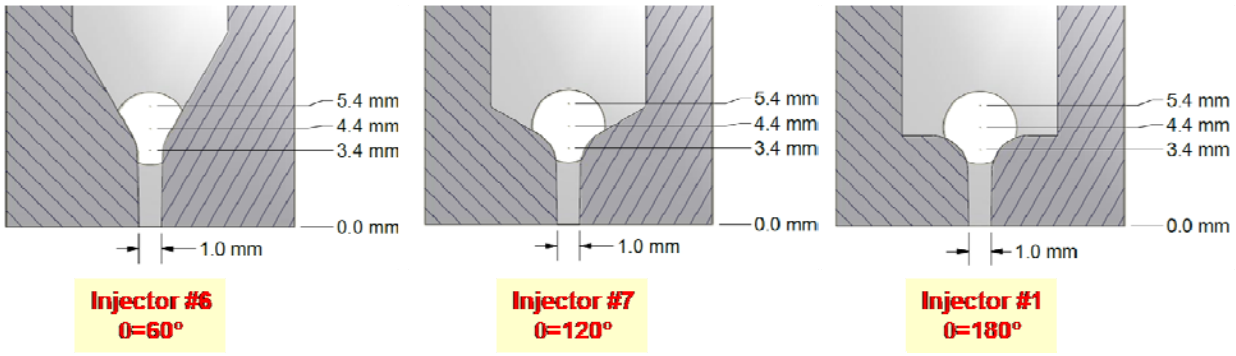

Figure 18 Schematic to illustrate the Window #1 location with respect to the Injector #1, #6 and #7 configurations.